Molecular Physics, 2013
Vol. 111, Nos. 12–13, 1781–1797, http://dx.doi.org/10.1080/00268976.2013.793835

Taylor & Francis
Taylor & Francis Group

INVITED ARTICLE

Interatomic potentials, electric properties and spectroscopy of the ground and excited states of the Rb_2 molecule: *ab initio* calculations and effect of a non-resonant field*

Michał Tomza[a,b], Wojciech Skomorowski[a], Monika Musiał[c], Rosario González-Férez[d], Christiane P. Koch[b] and Robert Moszynski[a,**]

[a]*Faculty of Chemistry, University of Warsaw, Warsaw, Poland;* [b]*Theoretische Physik, Universität Kassel, Kassel, Germany;* [c]*Institute of Chemistry, University of Silesia, Katowice, Poland;* [d]*Instituto Carlos I de Física Teórica y Computacional and Departamento de Física Atómica, Molecular y Nuclear, Universidad de Granada, Granada, Spain*

(*Received 21 January 2013; final version received 20 March 2013*)

We formulate the theory for a diatomic molecule in a spatially degenerate electronic state interacting with a non-resonant laser field and investigate its rovibrational structure in the presence of the field. We report on *ab initio* calculations employing the double electron attachment intermediate Hamiltonian Fock space coupled cluster method restricted to single and double excitations for all electronic states of the Rb_2 molecule up to $5s+5d$ dissociation limit of about 26,000 cm^{-1}. In order to correctly predict the spectroscopic behaviour of Rb_2, we have also calculated the electric transition dipole moments, non-adiabatic coupling and spin-orbit coupling matrix elements, and static dipole polarisabilities, using the multireference configuration interaction method. When a molecule is exposed to strong non-resonant light, its rovibrational levels get hybridised. We study the spectroscopic signatures of this effect for transitions between the $X^1\Sigma_g^+$ electronic ground state and the $A^1\Sigma_u^+$ and $b^3\Pi_u$ excited state manifold. The latter is characterised by strong perturbations due to the spin-orbit interaction. We find that for non-resonant field strengths of the order 10^9 W/cm^2, the spin-orbit interaction and coupling to the non-resonant field become comparable. The non-resonant field can then be used to control the singlet-triplet character of a rovibrational level.

Keywords: potential-energy curves; coupled-cluster theory; induced-dipole interaction; AC Stark effect; far-off-resonant laser field

1. Introduction

Rubidium was one of the first species to be Bose-condensed [1], and nowadays it can routinely be cooled and trapped. It has therefore become the drosophila of ultracold physics. Its long-range interatomic interactions have extensively been studied, and this has allowed to very accurately determine the scattering length and C_6 coefficient [2–4]. Rb_2 molecules have been formed out of ultracold rubidium atoms using both photo- and magneto-association [5,6]. Photoassociation and Feshbach spectroscopy have also served to measure the low-lying shape resonances of the rubidium dimer [7–9]. Trapping rubidium in an optical lattice has facilitated studies of atom-molecule dark states [10] and transferring the molecules into their vibrational ground state [11]. The Rb_2 molecule continues to draw attention in the context of the coherent control of ultracold collisions [12–16] and femtosecond photoassociation [17–20]. These experiments as well as those employing photoassociation with continuous wave lasers [21–25] require precise spectroscopic knowledge not only of the ground but also the excited states for both interpretation and detection.

The electronic ground and excited states have extensively been studied. According to Huber and Herzberg [26], the Rb_2 molecule was first observed in a spectroscopic experiment by Lawrence and Edlefsen as early as 1929 [27]. Cold molecule studies have led to a renewed interest in the Rb_2 molecule. The ground $X^1\Sigma_g^+$ state has been investigated in Ref. [28], while the most accurate experimental results for the $a^3\Sigma_u^+$ state have been reported by Lozeille *et al.* [29], Beser *et al.* [30] and Tiemann and collaborators [31]. The most important excited states corresponding to the $^2S+^2P$ dissociation limit, the $A^1\Sigma_u^+$ and $b^3\Pi_u$ states, have extensively been analysed in Ref. [21]. Less experimental information is available for other excited states. Notably, the $(1)^3\Sigma_g^+$ state has been studied in Ref. [32], and Ref. [33] reports the experimental observation of the $(2)^2\Pi_g$ state. The pure long-range state of 0_g^- symmetry, which is important for the photoassociation of ultracold Rb atoms, has been analysed in Ref. [34]. Several of these experimental data were successfully employed to derive empirical potentials that reproduce the spectroscopic data with the experimental accuracy (cf. Refs. [28,31] for the ground state $X^1\Sigma_g^+$ and

*This paper is dedicated to Professor Bretislav Friedrich on the occasion of his 60th birthday.

**Corresponding author. Email: robert.moszynski@tiger.chem.uw.edu.pl

Refs. [30,31] for the $a^3\Sigma_u^+$ potential). The coupled manifold of the $A^1\Sigma_u^+$ and $b^3\Pi_u$ states was deperturbed by Bergeman and collaborators [21,35] with the corresponding potential energy curves and spin-orbit coupling matrix elements reported in Ref. [35]. Potential energy curves for other electronic states fitted to the experimental data are older (cf. Ref. [36] for the empirical potential energy curve of the $(1)^1\Pi_g$ state, and Refs. [37] and [38] for those of the $(2)^1\Sigma_g^+$ state and $(2)^1\Pi_u$ states, respectively).

Given this extensive amount of experimental data, it is not surprising that many theoretical calculations have tackled the ground and excited states of the rubidium dimer. The first *ab initio* calculation on the Rb_2 molecule dates back to 1980 and was reported by Konowalow and Rosenkrantz [39]. Three recent studies have reported *ab initio* data of varying accuracy for the potential energy curves and in some cases further properties such as couplings and transition moments of Rb_2. The non-relativistic potentials for all molecular states by Park *et al.* [40] show a root mean square deviation (RMSD) between the theoretical well depths and the available experimental data of 235 cm^{-1}, i.e. 9.9% on the average. The 2003 calculations by Edvardsson *et al.* [41] were devoted to the ground state potential and six excited state potentials of ungerade symmetry. The spin-orbit coupling matrix elements were also reported. The overall accuracy of these results was about the same as in Ref. [40] with a RMSD of 180 cm^{-1} representing an average error of 25%. Note that since the number of states considered in Refs. [40] and [41] differs, the absolute RMSD may be smaller and the percentage error larger. Finally, in 2012, Allouche and Aubert-Frécon [42] reported calculations of all molecular states and spin-orbit coupling matrix elements corresponding to the dissociation limits $5s+5s$, $5s+5p$ and $5s+4d$. These calculations are much more accurate than any other previously reported in the literature with a RMSD of 129 cm^{-1}, i.e. an error of 5.5% only. However, they do not cover highly excited molecular states that are of interest for conventional spectroscopy experiments [43], for the detection of ultracold molecules [44] as well as photoassociation into states with ion-pair character [45–47].

Photoassociation into highly excited electronic states is at the core of a recent proposal for the production of ultracold Rb_2 molecules [47], aimed at improving earlier femtosecond experiments [17–20]. It is based on multi-photon transitions that can easily be driven by femtosecond laser pulses and allow to fully take advantage of the broad bandwidth of femtosecond laser pulses while driving the narrow photoassociation transition [48]. Moreover, multi-photon photoassociation populates highly excited electronic states with ion-pair character and strong spin-orbit interaction. These features are advantageous for an efficient stabilisation of the photoassociated molecules into deeply bound molecules in the electronic ground state [47]. The theoretical modelling of the proposed photoassociation scheme required the knowledge of precise *ab initio* potential energy curves including those for highly excited states, spin-orbit and non-adiabatic coupling matrix elements, electric transition dipole moments and dynamical Stark shifts. These data were not available in the literature for the highly excited states, and the non-adiabatic couplings and dynamical Stark shifts have been missing even for the lowest states. Moreover, the newly developed tools of electronic structure theory based on the Fock space coupled cluster method [49–51] could possibly allow for reaching a better accuracy of the potentials than reported in Refs. [40–42]. Last but not least, calculations of the electric properties for diatomic molecules in spatially degenerate electronic states are scarce. To the best of our knowledge, only two studies considered this problem, in the context of the dispersion interactions between molecules [52,53] rather than non-resonant interactions with an external field, and a systematic theoretical approach has not yet been proposed. Moreover, the presence of spin-orbit coupling between the electronic states has been neglected in a recent treatment of nuclear dynamics in a non-resonant field [54,55]. Such an approximation does not allow to study the competition between the spin-orbit coupling and the interaction with a non-resonant field, which may both significantly perturb the spectrum.

Here, we fill this gap and report the theoretical framework for a Π state molecule interacting with a non-resonant field and study its rovibrational dynamics in the presence of the field. We also report *ab initio* calculations of all potential energy curves, spin-orbit and non-adiabatic coupling matrix elements corresponding to the dissociation limits up to and including $5s+5d$. We test our *ab initio* results by comparing the main spectroscopic characteristics of the potentials to the available experimental data. We devote special emphasis to the important manifold of the $A^1\Sigma_u^+$ and $b^3\Pi_u$ states, comparing our results to Refs. [21,35]. Since the electric properties of spatially degenerate electronic states were not extensively studied in the literature thus far, we report here, to the best of our knowledge, the first *ab initio* calculation of the irreducible components of the polarisability tensor, including their dependence on the interatomic distance R, for the $A^1\Sigma_u^+$ and $b^3\Pi_u$ states. Finally, we study the effect of a non-resonant field on the spectroscopy in the $A^1\Sigma_u^+$ and $b^3\Pi_u$ manifold. This is motivated by our recent proposal for enhancing photoassociation by controlling shape resonances with non-resonant light [54,55]. In order to significantly modify the scattering continuum of the atom pairs to be photoassociated, rather large non-resonant intensities are required. Since the bound rovibrational levels are much more affected by a strong non-resonant field than continuum states, it is important to investigate how the corresponding spectroscopic features change.

Our paper is organised as follows. In Section 2, we formulate the theory of the interaction of a homonuclear molecule with an external non-resonant field. In Section 3,

we provide the theoretical description of the perturbation of spectra by a non-resonant field, using as an example the spin-orbit coupled manifold of the $A^1\Sigma_u^+$ and $b^3\Pi_u$ electronic states of Rb_2. We briefly summarise the *ab initio* methods employed in our calculations in Section 4 and discuss the results of these calculations in Section 5. In particular, we compare our data with results available in the literature and discuss the ability of the *ab initio* results to reproduce the high-resolution spectroscopic data for the $A^1\Sigma_u^+$ and $b^3\Pi_u$ manifold [21,35]. We then describe the interaction with a non-resonant field and study its spectroscopy signatures on the transitions between the electronic ground state and the $A^1\Sigma_u^+$ and $b^3\Pi_u$ manifold. Finally, Section 6 concludes our paper.

2. Diatomic molecule in a non-resonant electric field

We consider the interaction of a diatomic molecule with an electric field with the direction taken along the Z axis of the space-fixed coordinate system, $\vec{\mathcal{E}} = (0, 0, \mathcal{E})$. To the second order, the Hamiltonian for the interaction of the molecule with the electric field in the space-fixed frame can be written as,

$$H_{\rm int} = -d_Z^{\rm SF}\mathcal{E} - \frac{1}{2}\alpha_{ZZ}^{\rm SF}\mathcal{E}^2\,, \tag{1}$$

where $d_Z^{\rm SF}$ and $\alpha_{ZZ}^{\rm SF}$ denote, respectively, the appropriate components of the electric dipole moment and electric dipole polarisability in the space-fixed frame. Since we deal with a homonuclear molecule, only the second term of the above Hamiltonian will be relevant in the present analysis. To evaluate the matrix elements of the Hamiltonian in the electronic and rovibrational basis, we rewrite $\alpha_{ZZ}^{\rm SF}$ in terms of the polarisability components in the body-fixed frame. The $\alpha_{ZZ}^{\rm SF}$ dipole polarisability component can be expressed in terms of space-fixed irreducible tensor components $\alpha_m^{(l),{\rm SF}}$ [56],

$$\alpha_{ZZ}^{\rm SF} = -\frac{1}{\sqrt{3}}\alpha_0^{(0),{\rm SF}} + \sqrt{\frac{2}{3}}\alpha_0^{(2),{\rm SF}}\,. \tag{2}$$

For the irreducible tensor components, the transformation from the space-fixed to the body-fixed coordinate system is given by the rotation matrices $D_{m,k}^{(l)^\star}(\widehat{R})$,

$$\alpha_m^{(l),{\rm SF}} = \sum_{k=-l}^{l} D_{m,k}^{(l)^\star}(\widehat{R})\;\alpha_k^{(l),{\rm BF}}\,. \tag{3}$$

Hence, we have

$$\begin{aligned}\alpha_0^{(0),{\rm SF}} &= D_{0,0}^{(0)^\star}(\widehat{R})\;\alpha_0^{(0),{\rm BF}} = \alpha_0^{(0),{\rm BF}}\,,\\ \alpha_0^{(2),{\rm SF}} &= \sum_{k=-2}^{2} D_{0,k}^{(2)^\star}(\widehat{R})\;\alpha_k^{(2),{\rm BF}}\,.\end{aligned} \tag{4}$$

For simplicity, we omit the superscripts SF/BF in the rest of the paper as from now we will use only the body-fixed quantities. We assume in this paper that the molecular axis defines the body-fixed z axis. For a diatomic molecule, the set of the Euler angles $\widehat{R}$ can be chosen as $\widehat{R} = (0, \theta, 0)$, where θ is the angle between the molecular axis and the space-fixed Z axis. This particular choice of the Euler angles is consistent with the requirement that the space-fixed Y and body-fixed y axes coincide. The other possible set would be $\widehat{R} = (3\pi/2, \theta, \pi/2)$ that correspond to the coincidence of the space-fixed X and body-fixed x axes. Note that for our specific choice of the Euler angles, the Wigner D functions appearing in Equation (4) reduce to:

$$D_{0,k}^{(l)^\star}(\phi, \theta, 0) = \left[\frac{(l-k)!}{(l+k)!}\right]^{1/2} P_l^k(\cos\theta), \tag{5}$$

where P_l^k are the associated Legendre polynomials. For any diatomic molecule, the non-zero irreducible components of the dipole polarisability are $\alpha_0^{(0)}$ and $\alpha_0^{(2)}$. In addition, for a diatomic molecule in a Π electronic state, the $\alpha_{-2}^{(2)}$ and $\alpha_2^{(2)}$ terms do not vanish. They should be viewed as off-diagonal polarisability tensor components connecting two degenerate electronic states, $|\Pi_1\rangle$ and $|\Pi_{-1}\rangle$, with opposite projection of the total electronic orbital angular momentum on the molecular axis (see, for instance, Equation (16) of Ref. [53]).

The non-vanishing body-fixed polarisability components are most conveniently expressed in terms of the Cartesian tensor elements α_{ii}, $i = x, y, z$. Then $\alpha_0^{(0)}$ is related to the trace of the polarisability,

$$\alpha_0^{(0)} = -\frac{1}{\sqrt{3}}\left(\alpha_{xx} + \alpha_{yy} + \alpha_{zz}\right)\,, \tag{6}$$

$\alpha_0^{(2)}$ to the anisotropy of the polarisability,

$$\alpha_0^{(2)} = \frac{1}{\sqrt{6}}\left(2\alpha_{zz} - \alpha_{xx} - \alpha_{yy}\right)\,, \tag{7}$$

and, for a molecule in a Π electronic state, $\alpha_{-2}^{(2)}$ and $\alpha_2^{(2)}$ reflect the difference between two perpendicular components,

$$\alpha_2^{(2)} = \alpha_{-2}^{(2)} = \alpha_{yy} - \alpha_{xx}. \tag{8}$$

For a diatomic molecule in a Σ state, the definitions of the Cartesian components of the polarisability tensor α_{ii} in Equations (6)–(8) are unambiguous. The zz and xx components are simply the parallel and perpendicular components, $\alpha_\parallel$ and $\alpha_\perp$, respectively. Thus, the irreducible tensor components appearing in Equations (6)–(8) are simply related to the trace α and the anisotropy $\Delta\alpha$ of the polarisability

tensor,

$$\alpha_0^{(0)} = -\sqrt{3}\alpha, \qquad \alpha_0^{(2)} = \frac{2}{\sqrt{6}}\Delta\alpha\,. \tag{9}$$

Obviously, for a Σ state molecule, the xx and yy components are equal, and $\alpha_2^{(2)} = 0$.

In the case of a molecule in a degenerate electronic state (Π, Δ, etc.), some caution is needed when employing the Cartesian components α_{ii}, since one has to specify the basis of the electronic states, in which these quantities are expressed. Equation (8) assumes the Cartesian components, α_{yy} and α_{xx}, to be calculated for the $|\Pi_x\rangle$ state. However, the Cartesian basis $\{|\Pi_x\rangle, |\Pi_y\rangle\}$ for the Π electronic state is not convenient for the dynamical calculations, since the spin-orbit coupling matrix elements are complex in this basis. Therefore, we prefer to use the spherical basis $\{|\Pi_{-1}\rangle, |\Pi_1\rangle\}$ for the Π state over the Cartesian basis $\{|\Pi_x\rangle, |\Pi_y\rangle\}$ since it avoids complex quantities in the calculations and allows for a simple adaptation of the Hund's case (a) wave function to a given symmetry of the rovibrational level. Therefore, we will use the irreducible polarisability components $\alpha_m^{(l)}$ rather than the Cartesian α_{ii}.

Combining Equations (1)–(8) and making use of properties of the rotation matrices $D_{m,k}^{(l)^*}(\widehat{R})$, one arrives at the following Hamiltonian for the interaction of the homonuclear diatomic molecule with the static electric field,

$$H_{\rm int} = -\frac{\mathcal{E}^2}{2}\Bigg[-\frac{1}{\sqrt{3}}\alpha_0^{(0)} + \sqrt{\frac{2}{3}}\alpha_0^{(2)}P_2^0(\cos\theta) + \frac{1}{6}\alpha_2^{(2)}P_2^2(\cos\theta) + 4\alpha_{-2}^{(2)}P_2^{-2}(\cos\theta)\Bigg]. \tag{10}$$

The above Hamiltonian is valid for any isolated electronic state of a diatomic homonuclear molecule. Albeit, the last two terms in this equation are relevant only for molecules in a Π electronic state. Let us stress here that although this form of the Hamiltonian seems a bit elaborate at first glance, it simplifies the evaluation of the matrix elements in the symmetry-adapted basis set, and it also avoids any ambiguities when employing the Cartesian polarisability components for degenerate electronic states. Equation (10) also assumes the frequency of the non-resonant field to be far from any resonance that allows for using the static polarisability and the two-photon rotating-wave approximation. Such a field can be produced, for example, by a carbon dioxide laser with a wavelength of about 10 μm.

3. Hamiltonian for the Rb_2 molecule in the manifold of the coupled $A^1\Sigma_u^+$ and $b^3\Pi_u$ excited states interacting with a non-resonant field

We construct the Hamiltonian for the nuclear motion in Hund's case (a) coupling scheme with the primitive basis functions $|n, \Lambda\rangle|S, \Sigma\rangle|J, \Omega, M\rangle$ that are products of the electronic $|n, \Lambda\rangle$, electron spin $|S, \Sigma\rangle$ and rotational $|J, \Omega, M\rangle$ functions. Here, J is the total angular momentum quantum number, S is the total electronic spin quantum number, Λ and Σ are the projections of the total electronic orbital and total electronic spin angular momenta onto the molecular axis, and M is the projection of the total angular momentum onto the Z space-fixed axis. n labels the non-relativistic dissociation limit of the molecular state. We also define the projection of the total, electronic orbital plus spin, angular momentum onto the molecular axis, $\Omega = \Lambda + \Sigma$. For the coupled $A^1\Sigma_u^+$ and $b^3\Pi_u$ manifold, we consider the rovibrational levels of the e spectroscopic symmetry and odd parity. For simplicity, any hyperfine structure effects are neglected here. The properly symmetry-adapted Hund's case (a) wavefunctions read,

$$\begin{aligned}
|A^1\Sigma_{0_u^+}, J, M, e\rangle &= |A, 0\rangle|0, 0\rangle|J, 0, M\rangle\,,\\
|b^3\Pi_{0_u^+}, J, M, e\rangle &= \frac{1}{\sqrt{2}}\big[|b, 1\rangle|1, -1\rangle|J, 0, M\rangle\\
&\quad - |b, -1\rangle|1, 1\rangle|J, 0, M\rangle\big]\,,\\
|b^3\Pi_{2_u}, J, M, e\rangle &= \frac{1}{\sqrt{2}}\big[|b, 1\rangle|1, 1\rangle|J, 2, M\rangle\\
&\quad - |b, -1\rangle|1, -1\rangle|J, -2, M\rangle\big]\,.
\end{aligned} \tag{11}$$

The first two states have a projection of the total angular momentum onto the molecular axis $|\Omega| = 0$, while the third one has $|\Omega| = 2$. In the field-free case, the state with $|\Omega| = 2$ is decoupled from the states with $|\Omega| = 0$, and it is not accessible from the ground electronic state in the one-photon dipolar transitions considered here. Consequently, the field-free model Hamiltonian H_0 describing the nuclear motion in the manifold of the coupled $A^1\Sigma_u^+$ and $b^3\Pi_u$ states can be represented by following 2×2 matrix,

$$H_0 = \begin{pmatrix} T_R + \frac{\vec{j}^2}{2\mu R^2} + V^{A^1\Sigma_u^+}(R) & \xi_1(R) \\ \xi_1(R) & T_R + \frac{\vec{j}^2}{2\mu R^2} + V^{b^3\Pi_u}(R) - \xi_2(R) \end{pmatrix}, \tag{12}$$

where $T = T_R + \frac{\vec{j}^2}{2\mu R^2}$ is the sum of the vibrational and rotational kinetic energy operators with $\vec{j} = \vec{J} - \vec{L} - \vec{S}$ being the mechanical angular momentum of the molecule and $V^k(R)$, $k = A^1\Sigma_u^+$, $b^3\Pi_u$, denotes the respective potential energy curves in the Born-Oppenheimer approximation. $\xi_1(R) = \langle A^1\Sigma_u^+|H_{\rm SO}|b^3\Pi_u\rangle_{|\Omega|=0}$ and $\xi_2(R) = \langle b^3\Pi_u|H_{\rm SO}|b^3\Pi_u\rangle_{|\Omega|=0}$ are the spin-orbit coupling matrix elements, and only the electronic states with $|\Omega| = 0$ are included. Our model does not account for Coriolis-type

angular couplings, i.e. the couplings of the $\Omega = 0$ states with $\Omega = 1$ states because their effect on the rovibrational dynamics is negligible compared to the spin-orbit couplings, the error of the electronic structure data and the influence of the weak non-resonant field. It is not surprising due to large reduced mass of Rb_2 molecules whose inverse enters all coupling matrix elements.

When the electric field is switched on, the $\Lambda = 1$ and $\Lambda = -1$ components of the $b^3\Pi_u$ state are coupled. The coupling results form the off-diagonal polarisability tensor components in the Hamiltonian of Equation (10). Therefore, not only the interaction $H_{\rm int}$ from Equation (10) has to be added to the Hamiltonian H_0 for the $A^1\Sigma_u^+$ and $b^3\Pi_u$ states with $|\Omega| = 0$, but also the matrix (12) has to be extended so as to include the $|\Omega| = 2$ component originating from the $b^3\Pi_u$ state since it has the Λ projections exactly opposite to those found in the state with $|\Omega| = 0$ while all other quantum numbers are the same. Hence, in the presence of the electric field the rovibrational levels of the $A\,^1\Sigma_u^+$ and $b^3\Pi_u$ manifold are obtained by diagonalising the Hamiltonian represented by the following 3×3 matrix,

$$H = \begin{pmatrix} T + W^{A^1\Sigma_u^+}(R,\theta) & \xi_1(R) & 0 \\ \xi_1(R) & T + W^{b^3\Pi_u}(R,\theta) - \xi_2(R) & W_{0/2}(R,\theta) \\ 0 & W_{0/2}(R,\theta) & T + W^{b^3\Pi_u}(R,\theta) + \xi_2(R) \end{pmatrix}. \qquad (13)$$

The diagonal elements of the interaction potentials incorporating the interaction with non-resonant field are given by,

$$W^k(R,\theta) = V^k(R) + H^k_{\rm int}\,, \qquad (14)$$

where $k = A^1\Sigma_u^+$ or $b^3\Pi_u$ and $H^k_{\rm int}$ is given by Equation (10) for the electronic state labelled by k. The off-diagonal term due to the non-resonant field, $W_{0/2}(R,\theta)$, couples the $|\Omega| = 0_u^+$ and $|\Omega| = 2_u$ components resulting from the $b^3\Pi_u$ state. It is proportional to the off-diagonal polarisability of the molecule in the $b^3\Pi$ state,

$$W_{0/2}(R,\theta) = -\frac{1}{12}\mathcal{E}^2\alpha_2^{(2),b^3\Pi_u}(R)P_2^2(\cos\theta)\,, \qquad (15)$$

with $\alpha_2^{(2)}$ defined by Equation (8). Analogously to Equations (13) and (14), the Hamiltonian for the molecule in its electronic ground state interacting with a non-resonant field is simply given by $T + W^{X^1\Sigma_g^+}(R,\theta)$.

4. *Ab initio* electronic structure and dynamical calculations

We adopt the computational scheme successfully applied to the ground and excited states of the calcium dimer [57–61], magnesium dimer [62,63], strontium dimer [64,65], $(BaRb)^+$ molecular ion [66] and SrYb heteronuclear molecule [67]. The potential energy curves for the singlet and triplet gerade and ungerade states of the Rb_2 molecule corresponding to the first seven lowest dissociation limits, $5s+5s$, $5s+5p$, $5s+4d$, $5s+6s$, $5s+6p$, $5p+5p$ and $5s+5d$, have been obtained by a supermolecule method,

$$V^{^{2S+1}|\Lambda|_{g/u}}(R) = E^{\rm SM}_{\rm AB} - E^{\rm SM}_{\rm A} - E^{\rm SM}_{\rm B}\,, \qquad (16)$$

where $E^{\rm SM}_{\rm AB}$ denotes the energy of the dimer computed using the supermolecule method (SM), and $E^{\rm SM}_X$, $X = A$ or B, is the energy of the atom X in the electronic state corresponding to the dissociation limit of the state $^{2S\,+\,1}|\Lambda|_{g/u}$. The full basis of the dimer was employed in the supermolecule calculations on the atoms A and B, and the molecule AB, and the Boys and Bernardi scheme was utilised to correct for the basis-set superposition error [68]. The calculations for the excited states employed the recently introduced double electron attachment intermediate Hamiltonian Fock space coupled cluster method restricted to single and double excitations (DEA-IH-FS-CCSD) [49,51]. Starting with the closed-shell reference state for the doubly ionised molecule Rb_2^{2+} that shows the correct dissociation at large interatomic separations, R, into closed-shell subsystems, $Rb^+ + Rb^+$, and using the double electron attachment operators in the Fock space coupled cluster ansatz makes our method size-consistent at any interatomic separation R and guarantee the correct large-R asymptotics. Thus, the DEA-IH-FS-CCSD approach overcomes the problem of the standard coupled cluster method restricted to single and double excitations (CCSD) and the equation of motion CCSD method [50] with the proper dissociation into open-shell atoms. The potential energy curves obtained from the *ab initio* calculations were smoothly connected at intermediate interatomic separations with the asymptotic multipole expansion [56]. The C_6 coefficient of the electronic ground state and the C_3 coefficient of the first excited state were fixed at their empirical values derived from high-resolution spectroscopic experiments [4,34], while the remaining coefficients were taken from Ref. [69].

The transitions from the ground $X^1\Sigma_g^+$ state to the $^1\Sigma_u^+$ and $^1\Pi_u$ states and from the $a^3\Sigma_u^+$ to the $^3\Sigma_g^+$ and $^3\Pi_g$ states are electric dipole allowed. The transition dipole moments for the electric transitions were computed from the following expression [70],

$$\begin{aligned} d_i(n \leftarrow X) &= \left\langle X^1\Sigma_g^+ \middle| \hat{d}_i \middle| (n)^1|\Lambda|_u \right\rangle \\ d_i(n \leftarrow a) &= \left\langle a^3\Sigma_u^+ \middle| \hat{d}_i \middle| (n)^3|\Lambda|_g \right\rangle, \end{aligned} \qquad (17)$$

where the $\hat{d}_i$, $i = x, y$ or z, denotes the ith component of the electric dipole moment operator. Note that in the first term

of Equation (17) $i = x$ or y corresponds to transitions to $^1\Pi_u$ states, while $i = z$ corresponds to transitions to $^1\Sigma_u^+$ states. The transitions from the $a^3\Sigma_u^+$ state connect this state with the $^3\Pi_g$ and $^3\Sigma_g^+$ states, through the x or y and z operators, respectively.

We expect the rovibrational energy levels of the excited electronic states of Rb_2 to show perturbations due to the non-adiabatic couplings between the states. Analysing the pattern of the potential energy curves, we have found that many potential energy curves display avoided crossings, suggesting strong radial couplings between these electronic states. We have therefore computed the most important radial coupling matrix elements, defined by the expression,

$$R(n \leftrightarrow n') = \left\langle (n)^{2S+1}|\Lambda|_{g/u} \left| \frac{\partial}{\partial R} \right| (n')^{2S+1}|\Lambda|_{g/u} \right\rangle , \tag{18}$$

where $n \leftrightarrow n'$ signifies that the electronic states n and n' are coupled. Note that the radial derivative operator couples states with the same projection of the electronic orbital angular momentum on the molecular axis Λ.

Electric transition dipole moments, radial non-adiabatic coupling and spin-orbit coupling matrix elements were obtained using the Multireference Configuration Interaction (MRCI) method restricted to single and double excitations with a large active space. Scalar relativistic effects were included by using the small-core fully relativistic energy-consistent pseudopotential ECP28MDF [71] from the Stuttgart library. Thus, in the present study, the Rb_2 molecule was treated as a system of effectively 18 electrons. The [14*s*14*p*7*d*6*f*] basis set was employed in all calculations. This basis was obtained by decontracting and augmenting the basis set of Ref. [71] by a set of additional functions improving the accuracy of the atomic excitation energies of the rubidium atom with respect to the NIST database [72]. The DEA-IH-FS-CCSD calculations were done with the code based on the ACES II program system [73], while the MRCI calculations were performed with the MOLPRO code [74]. All *ab initio* results reported in the present paper are available from the Authors on request.

The rovibrational levels of the $A^1\Sigma_u^+$ and $b^3\Pi_u$ excited state manifold are computed by diagonalising the Hamiltonian (12) represented on a mapped Fourier grid, employing about $N_R = 512$ radial grid points. For the calculations in the field we complement our Fourier grid representation for the radial part by a basis set expansion in terms of Legendre polynomials for the angular part, taking advantage of the magnetic quantum number m being conserved. We find that $j_{max} = 19$ is sufficient to obtain converged results for $\mathcal{I} \leq 2 \times 10^9$ W/cm^2. Presence of an intense non-resonant field leads to strong hybridisation of the rovibrational levels, and an adiabatic separation of rotational and vibrational motion is not applicable [54,55]. We account for this fact by diagonalising the full two-dimensional Hamiltonian, Equation (13), represented by a $3N_R(j_{max} + 1) \times 3N_R(j_{max} + 1)$ matrix. For $\mathcal{I} \neq 0$, the non-resonant field mixes different partial waves, and j and j' are not good quantum numbers anymore. For the sake of simplicity, we label the field-dressed rovibrational levels by the field-free quantum numbers. Note that the field-dressed levels are adiabatically connected to their field-free counterparts even for very large intensities.

5. Numerical results and discussion

5.1. Potential energy curves

To test the ability of the *ab initio* approach adopted in the present work to reproduce the experimental data, we first check the accuracy of the atomic results. In Table 1, we report the excitation energies at the dissociation limit computed with the DEA-IH-FS-CCSD method and compare the results to non-relativistic excitation energies

Table 1. Asymptotic energies (in cm^{-1}) and molecular states arising from different states of rubidium atoms [26].

Asymptote	Energy (Present)	Energy (Exp.)	Molecular states
$(1)^2S(5s)+(1)^2S(5s)$	0	0	$^1\Sigma_g^+$, $^3\Sigma_u^+$
$(1)^2S(5s)+(1)^2P(5p)$	12731	12737	$^1\Sigma_g^+$, $^1\Pi_g$, $^1\Sigma_u^+$, $^1\Pi_u$, $^3\Sigma_g^+$, $^3\Pi_g$, $^3\Sigma_u^+$, $^3\Pi_u$
$(1)^2S(5s)+(1)^2D(4d)$	19471	19355	$^1\Sigma_g^+$, $^1\Sigma_u^+$, $^1\Pi_g$, $^1\Pi_u$, $^1\Delta_g$, $^1\Delta_u$, $^3\Sigma_g^+$, $^3\Sigma_u^+$, $^3\Pi_g$, $^3\Pi_u$, $^3\Delta_g$, $^3\Delta_u$
$(1)^2S(5s)+(2)^2S(6s)$	20126	20133	$^1\Sigma_g^+$, $^1\Sigma_u^+$, $^3\Sigma_g^+$, $^3\Sigma_u^+$
$(1)^2S(5s)+(2)^2P(6p)$	23732	23767	$^1\Sigma_g^+$, $^1\Pi_g$, $^1\Sigma_u^+$, $^1\Pi_u$, $^3\Sigma_g^+$, $^3\Pi_g$, $^3\Sigma_u^+$, $^3\Pi_u$
$(1)^2P(5p)+(1)^2P(5p)$	25462	25475	$^1\Sigma_g^+(2)$, $^1\Sigma_u^-$, $^1\Pi_g$, $^1\Pi_u$, $^1\Delta_g$, $^3\Sigma_u^+(2)$, $^3\Sigma_g^-$, $^3\Pi_g$, $^3\Pi_u$, $^3\Delta_u$
$(1)^2S(5s)+(2)^2D(5d)$	25736	25707	$^1\Sigma_g^+$, $^1\Sigma_u^+$, $^1\Pi_g$, $^1\Pi_u$, $^1\Delta_g$, $^1\Delta_u$, $^3\Sigma_g^+$, $^3\Sigma_u^+$, $^3\Pi_g$, $^3\Pi_u$, $^3\Delta_g$, $^3\Delta_u$
$Rb^+(^1S)+Rb^-(^1S)$	29741	29771	$^1\Sigma_g^+$, $^1\Sigma_u^+$

obtained with the Landé rule from the experimental excitation energies. Inspection of Table 1 shows that the agreement between the theoretical and experimental excitation energies is very good. For the $5s+ns$ and $5s+np$ dissociation limits, the RMSD is only 21 cm^{-1}, which represents an error of 0.08%. When the D states are included, this good agreement is somewhat degraded. The RMSD is now 49 cm^{-1}, i.e. 0.26%. This is due to the lack of g symmetry functions in the basis set used in our calculations. Note parenthetically that we could not include g functions in the basis, because the ACESS II program does not support g orbitals in the calculations involving pseudopotentials. Our method reproduces very well the electron affinity of the Rb atom, 3893 cm^{-1} on the theory side versus 3919 cm^{-1} measured in Ref. [75], as well as the ionisation potential, 33630 cm^{-1} versus 33690 cm^{-1} [72]. Finally, we note that the ground state static electric dipole polarisability of the atom obtained from our molecular calculations is 319.5 a_0^3 compared to 318.6 a_0^3 from the most sophisticated atomic calculations by Derevianko *et al.* [76].

The computed potential energy curves are reported in Figure 1 for the $^1\Sigma_g^+$ and $^3\Sigma_g^+$ symmetries, in Figure 2 for the $^1\Sigma_u^+$ and $^3\Sigma_u^+$ symmetries, in Figures 3 and 4 for the $^1\Pi_g$ and $^3\Pi_g$, and $^1\Pi_u$ and $^3\Pi_u$ symmetries, respectively. Finally, Figure 5 shows the potential energy curves for the singlet and triplet gerade and ungerade states of Δ symmetry. The spectroscopic characteristics of the singlet gerade states are reported in Table 2 while Table 3 collects these properties for the triplet gerade states. Tables 4 and 5 present

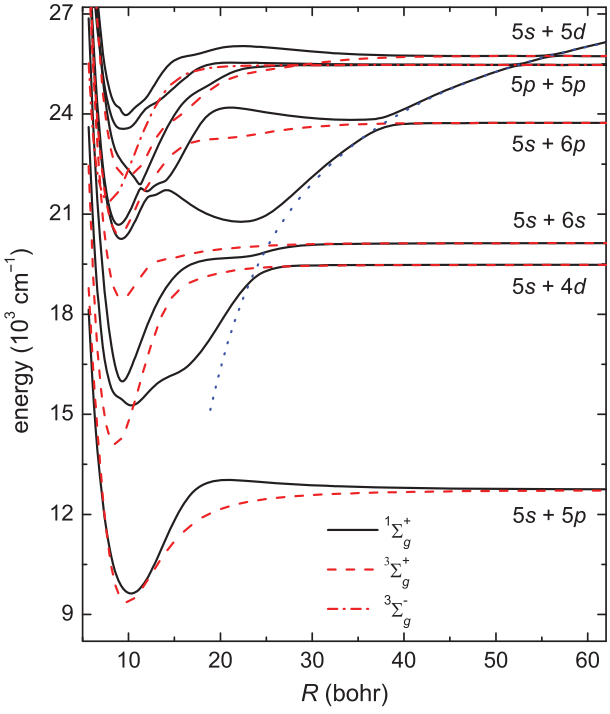

Figure 1. Potential energy curves for the $^1\Sigma_g^+$ and $^3\Sigma_g^\pm$ states of the Rb_2 molecule.

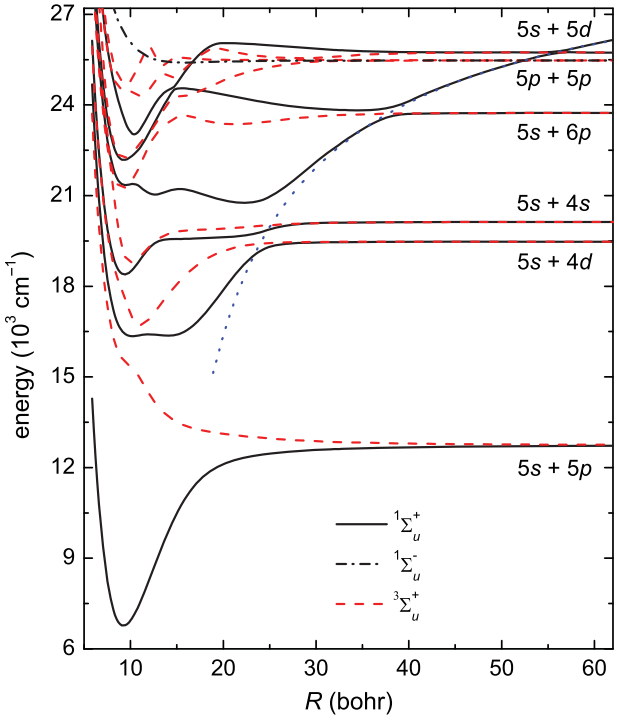

Figure 2. Potential energy curves for the $^1\Sigma_u^\pm$ and $^3\Sigma_u^+$ states of the Rb_2 molecule.

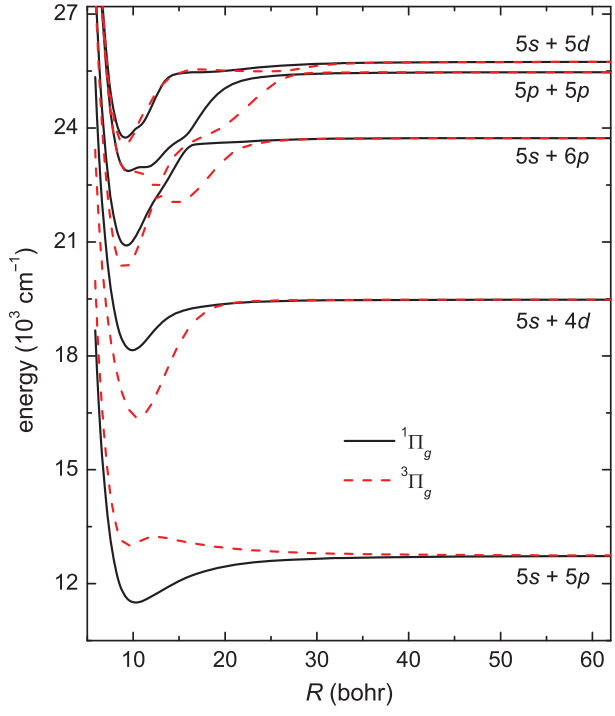

Figure 3. Potential energy curves for the $^1\Pi_g$ and $^3\Pi_g$ states of the Rb_2 molecule.

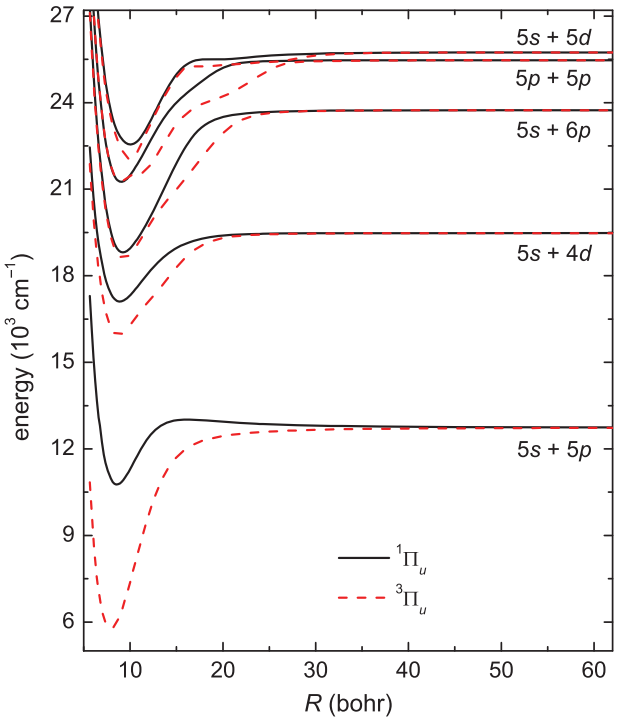

Figure 4. Potential energy curves for the $^1\Pi_u$ and $^3\Pi_u$ states of the Rb_2 molecule.

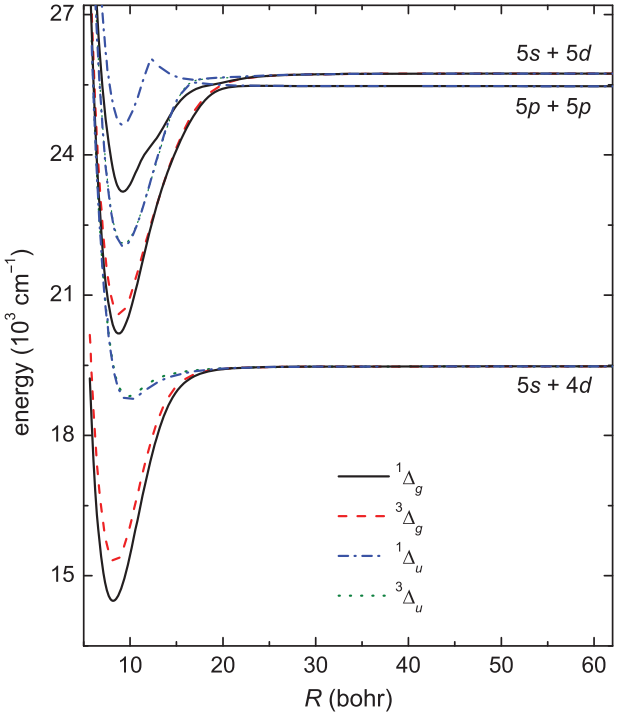

Figure 5. Potential energy curves for the $^1\Delta_{g/u}$ and $^3\Delta_{g/u}$ states of the Rb_2 molecule.

the results for the singlet and triplet states of ungerade symmetry, respectively. Inspection of Figures 1–5 reveals that almost all potential energy curves show a smooth behaviour with well-defined minima. Some higher states display perturbations, mostly in the form of avoided crossings, due to the interaction with other electronic states of the same symmetry that are located nearby. At high energies, the density of states becomes so high that the avoided crossings produce some irregularities in the curves. This is especially true for the singlet and triplet gerade and ungerade states of Σ^+ symmetry. The Π states show less perturbations, except for the avoided crossings between the curves corresponding to the $(3)^1\Pi_g$ and $(4)^1\Pi_g$, and $(3)^3\Pi_g$ and $(4)^3\Pi_g$ states. Interestingly, the Π_u states and the Δ states do not show any irregularity due to non-adiabatic interactions between the states.

The agreement of the present potentials with those derived from the experimental data is very good. This is demonstrated in Tables 2–5, where we compare the potential characteristics with the available experimental data and with the most recent calculations [42]. For all the experimentally observed states, the RMSD of our calculation is only 75.9 cm^{-1}, i.e. the error is 3.2% on average, better than the most recent calculations by Allouche and Aubert-Frécon [42] with a RMSD of 129 cm^{-1} corresponding to an average error of 5.5%. It is gratifying to observe that we reproduce low lying and highly excited electronic states equally well. This is in a sharp contrast to Ref. [42], which reproduces the well depth of the $(2)^1\Pi_u$ state only with an error of 12% compared to 3.5% for our calculation. Such a good agreement between theory and experiment for the highest observed excited electronic state gives us confidence that our predictions for the photoassociative production of ultracold Rb_2 molecules in even higher electronic states [47] are accurate. Tables 2–5 also report the fundamental vibrational frequencies ω_e for all electronic states considered in the present paper. Except for the ground state, the agreement between theory and experiment is within a few tenths of a wavenumber. Similar agreement was found in the calculations by Allouche and Aubert-Frécon [42].

5.2. *Non-adiabatic coupling and spin-orbit coupling matrix elements*

The importance of non-adiabatic interactions between electronic states, resulting in the avoided crossings of the corresponding potential energy curves observed in Figures 1–5, can nicely be explained by analysing the non-adiabatic coupling matrix elements computed according to Equation (18). The non-adiabatic coupling matrix elements are reported in Figure 6 for singlet and triplet states of Σ_g^+ and Σ_u^+ symmetry (top) and the Π states (bottom). As expected, the non-adiabatic coupling matrix elements are smooth, Lorenzian-type functions, which, in the limit of an infinitely close avoided crossing, become a Dirac

Table 2. Spectroscopic characteristics of the non-relativistic $^1|\Lambda|_g$ electronic states of $^{87}Rb_2$ molecule.

State	Ref.	R_e (Bohr)	D_e (cm^{-1})	ω_e (cm^{-1})	T_e (cm^{-1})	Asymptote
$X^1\Sigma_g^+$	Present	7.99	3912	56.1	0	$5s+5s$
	[28] (Exp.)	7.96	3994	57.8	0	
	[42]	7.96	3905	58.4	0	
$(2)^1\Sigma_g^+$	Present	10.29	3102	32.0	13545	$5s+5p$
	[37] (Exp.)	10.28	2963	31.5	13602	
	[42]	10.17	3084	31.2	13559	
$(3)^1\Sigma_g^+$	Present	10.32	4210	32.9	19180	$5s+4d$
	[42]	10.20	4072	31.9	19189	
$(4)^1\Sigma_g^+$	Present	9.34	4144	62.0	19898	$5s+6s$
$(5)^1\Sigma_g^+$	Present	9.21	3483	37.8	24166	$5s+6p$
2nd min.	Present	22.22	2968	11.0	24681	
$(6)^1\Sigma_g^+$	Present	8.93	3055	46.6	24594	$5s+5p$
2nd min.	Present	12.02	2056	50.6	25593	
3rd min.	Present	34.60	86	4.7	27734	
$(7)^1\Sigma_g^+$	Present	11.26	1852	92.8	25797	$5s+5p$
$(8)^1\Sigma_g^+$	Present	9.47	183	41.3	27465	$5s+5d$
$(1)^1\Pi_g$	Present	10.25	1230	21.7	15417	$5s+5p$
	[36] (Exp.)	10.24	1290	22.3	15510	
	[42]	10.24	1198	22.0	15545	
$(2)^1\Pi_g$	Present	9.92	1326	31.0	22063	$5s+4d$
	[42]	9.88	1238	22.0	22023	
$(3)^1\Pi_g$	Present	9.25	2833	43.1	22149	$5s+6p$
$(4)^1\Pi_g$	Present	9.48	2598	37.1	22099	$5p+5p$
$(5)^1\Pi_g$	Present	9.13	1994	42.9	22187	$5s+5d$
$(1)^1\Delta_g$	Present	8.18	5026	48.7	18449	$5s+4d$
	[42]	8.14	4871	50.5	18390	
$(2)^1\Delta_g$	Present	8.76	5291	57.6	24165	$5p+5p$
$(3)^1\Delta_g$	Present	9.22	2528	56.5	27212	$5s+5d$

Table 3. Spectroscopic characteristics of the non-relativistic $^3|\Lambda|_g$ electronic states of $^{87}Rb_2$ molecule.

State	Ref.	R_e (Bohr)	D_e (cm^{-1})	ω_e (cm^{-1})	T_e (cm^{-1})	Asymptote
$(1)^3\Sigma_g^+$	Present	9.91	3367	37.8	13279	$5s+5p$
	[42]	9.73	3345	36.6	13298	
$(2)^3\Sigma_g^+$	Present	8.58	5372	51.1	18017	$5s+4d$
	[42]	8.47	5347	51.5	17914	
$(3)^3\Sigma_g^+$	Present	9.31	1657	38.2	22384	$5s+6s$
$(4)^3\Sigma_g^+$	Present	8.95	3335	46.7	24313	$5s+6p$
$(5)^3\Sigma_g^+$	Present	9.72	3488	19.4	26065	$5p+5p$
$(6)^3\Sigma_g^+$	Present	9.19	3292	43.8	26953	$5s+5p$
$(7)^3\Sigma_g^+$	Present	9.12	3268	38.5	27832	$5s+5d$
$(1)^3\Pi_g$	Present	9.54	−267	30.3	16914	$5s+5p$
	[42]	9.47	−268	30.3	16911	
$(2)^3\Pi_g$	Present	10.56	3104	34.2	20285	$5s+4d$
	[42]	10.53	2927	33.6	20334	
$(3)^3\Pi_g$	Present	9.08	3416	45.4	24232	$5s+6p$
$(4)^3\Pi_g$	Present	9.06	2646	27.4	26735	$5p+5p$
$(5)^3\Pi_g$	Present	9.09	2170	45.8	27484	$5s+5d$
$(1)^3\Delta_g$	Present	8.36	4181	48.3	19284	$5s+4d$
	[42]	8.31	4017	48.9	19244	
$(2)^3\Delta_g$	Present	8.85	5152	46.2	24588	$5s+5d$

Table 4. Spectroscopic characteristics of the non-relativistic $^1|\Lambda|_u$ electronic states of $^{87}Rb_2$ molecule.

State	Ref.	R_e (Bohr)	D_e (cm^{-1})	ω_e (cm^{-1})	T_e (cm^{-1})	Asymptote
$A^1\Sigma_u^+$	Present	9.24	5967	44.1	10680	$5s+5p$
	[35] (Exp.)	9.21	5981	44.6	10750	
	[42]	9.20	5896	44.4	10747	
$(2)^1\Sigma_u^+$	Present	10.21	3128	20.5	20261	$5s+4d$
	[42]	10.09	3003	22.1	20258	
2nd min.	Present	14.11	3112	13.5	20277	
	[42]	13.81	2926	11.5	20335	
$(3)^1\Sigma_u^+$	Present	9.37	1737	42.4	22305	$5s+6s$
$(4)^1\Sigma_u^+$	Present	9.46	2390	31.3	25258	$5s+6p$
2nd min.	Present	12.64	2702	24.3	24946	
3rd min.	Present	22.26	2973	10.7	24675	
$(5)^1\Sigma_u^+$	Present	9.28	3565	39.1	26088	$5p+5p$
2nd min.	Present	34.69	1920	5.0	27733	
$(6)^1\Sigma_u^+$	Present	10.38	3308	52.9	26937	$5s+5d$
$(1)^1\Pi_u$	Present	8.57	1971	46.9	14676	$5s+5p$
	[38] (Exp.)	–	1907	47.5	14666	
	[42]	8.48	1989	47.9	14654	
$(2)^1\Pi_u$	Present	8.92	2369	31.6	21021	$5s+4d$
	[38] (Exp.)	–	2454	36.4	20895	
	[42]	8.77	2157	36.1	21104	
$(3)^1\Pi_u$	Present	9.23	4927	40.4	22721	$5s+6p$
$(4)^1\Pi_u$	Present	9.03	4216	43.1	25166	$5p+5p$
$(5)^1\Pi_u$	Present	10.06	3189	31.4	26465	$5s+5d$
$(1)^1\Delta_u$	Present	9.80	639	28.0	22825	$5s+4d$
	[42]	9.78	542	26.9	22718	
$(2)^1\Delta_u$	Present	9.31	3638	48.1	25818	$5p+5p$
$(3)^1\Delta_u$	Present	9.40	2630	34.2	27110	$5s+5d$

Table 5. Spectroscopic characteristics of the non-relativistic $^3|\Lambda|_u$ electronic states of $^{87}Rb_2$ molecule.

State	Ref.	R_e (Bohr)	D_e (cm^{-1})	ω_e (cm^{-1})	T_e (cm^{-1})	Asymptote
$a^3\Sigma_u^+$	Present	11.46	250	13.5	3662	$5s+5s$
	[31] (Exp.)	11.51	242	13.5	–	
	[42]	11.45	237	13.3	3669	
$(2)^3\Sigma_u^+$	Present	repulsive	–	–	–	$5s+5p$
$(3)^3\Sigma_u^+$	Present	11.02	2761	40.0	20628	$5s+4d$
	[42]	10.96	2646	40.6	20614	
$(4)^3\Sigma_u^+$	Present	10.06	1340	43.0	22701	$5s+6s$
$(5)^3\Sigma_u^+$	Present	9.18	2493	44.7	25155	$5s+6p$
$(6)^3\Sigma_u^+$	Present	9.29	3235	40.9	26147	$5p+5p$
$(7)^3\Sigma_u^+$	Present	9.09	938	47.2	28444	$5p+5p$
$b^3\Pi_u$	Present	7.91	6969	57.2	9677	$5s+5p$
	[35] (Exp.)	7.81	7039	60.1	9601	
	[42]	7.88	7015	59.7	9624	
$(2)^3\Pi_u$	Present	8.73	3527	43.5	19862	$5s+4d$
	[42]	8.60	3497	43.3	19764	
$(3)^3\Pi_u$	Present	9.28	5117	40.0	22531	$5s+6p$
$(4)^3\Pi_u$	Present	8.99	4189	43.3	25193	$5p+5p$
$(5)^3\Pi_u$	Present	10.04	3711	56.5	25943	$5s+5d$
$(1)^3\Delta_u$	Present	9.83	719	27.3	22746	$5s+4d$
	[42]	9.86	619	25.8	22641	
$(2)^3\Delta_u$	Present	9.30	3695	40.7	25761	$5s+5d$

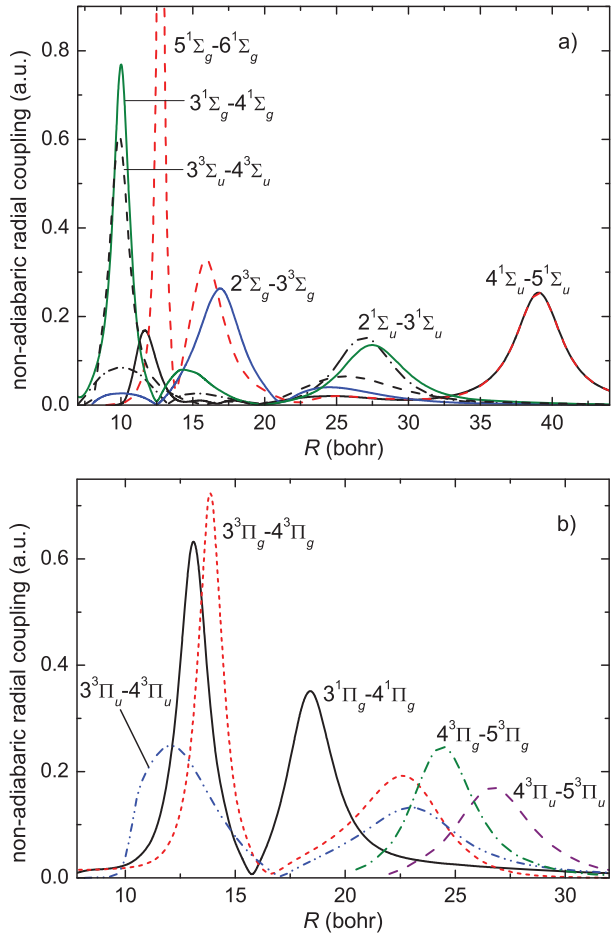

Figure 6. Non-adiabatic radial coupling matrix elements between states of Σ (*a*) and Π (*b*) symmetry.

δ-function. The height and width of the curve depends on the strength of the interaction. The smaller the width and the larger the peak, the stronger is the interaction between the electronic states, and the corresponding potential energy curves are closer to each other at the avoided crossing. It is gratifying to observe that the maxima on the non-adiabatic coupling matrix elements agree well with the locations of the avoided crossing, and this despite the fact that two very different methods were used in *ab initio* calculations. Since the potential energy curves were shown to be accurate, cf. the discussion in Section 5.1, we are confident that also the non-adiabatic coupling matrix elements are essentially correct.

Rubidium is a heavy atom and the electronic states of the Rb_2 molecule show strong couplings due to the relativistic spin-orbit interaction. Figure 7 reports the spin-orbit coupling matrix elements as a function of the interatomic separation. The matrix elements are all represented by smooth curves approaching the atomic limit at large *R*. The fine splittings of the atomic states are very accurately reproduced by our calculations. For the first excited P state, the theoretical splitting between the 1/2 and 3/2

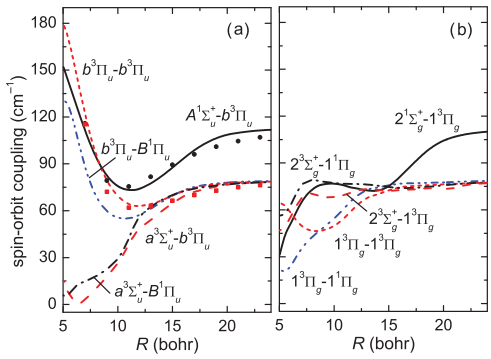

Figure 7. Spin-orbit coupling matrix elements between states of ungerade (*a*) and gerade (*b*) symmetries dissociating into $^2S(5s) + {}^2P(5p)$. Black circles and red squares are analytical fit to high-resolution spectroscopic data from Ref. [35].

components is 236.2 cm^{-1} as compared to 237.6 cm^{-1} from the experiment. It is also gratifying to observe that our *ab initio* calculations reproduce very well the spin-orbit coupling functions obtained from fitting analytical functions to high-resolution spectroscopic data for the $A^1\Sigma_u^+$ and $b^3\Pi_u$ manifold of states [35]. This gives us confidence that also perturbations in the molecular spectra due to the spin-orbit interaction will correctly be reproduced from the present *ab initio* data.

5.3. *Electric transition dipole moments and electric dipole polarisabilities*

A full characterisation of the molecular spectra requires knowledge of the electric transition dipole moments. These were calculated according to Equation (17) and are presented in Figure 8 for transitions from the $X^1\Sigma_g^+$ ground state and in Figure 9 for transitions from the $a^3\Sigma_u^+$ lowest triplet state. The strongest transitions from the ground singlet state are those to the $A^1\Sigma_u^+$ and $(1)^1\Pi_u$ states, i.e. to states corresponding to the first excited dissociation limit. All other transition moments are much smaller, suggesting that the corresponding line intensities in the spectra will be much weaker. The same is true for transitions departing from the $a^3\Sigma_u^+$ state. The transition moments do not show a strong dependence on *R*, except at small interatomic separations, and smoothly tend to their asymptotic atomic value.

The static electric dipole polarisabilities for the $X^1\Sigma_g^+$ electronic ground state, the $a^3\Sigma_u^+$ state and the relevant excited $A^1\Sigma_u^+$ and $b^3\Pi_u$ states are presented in Figure 9. They show an overall smooth behaviour and also tend smoothly to their asymptotic atomic values. The interaction-induced variation of the polarisability is clearly visible while changing the internuclear distance *R*. It is significant for excited states, especially for the $A^1\Sigma_u^+$ state for which the isotropic part α reaches 8000 a_0^3, and the anisotropic part $\Delta\alpha$ reaches

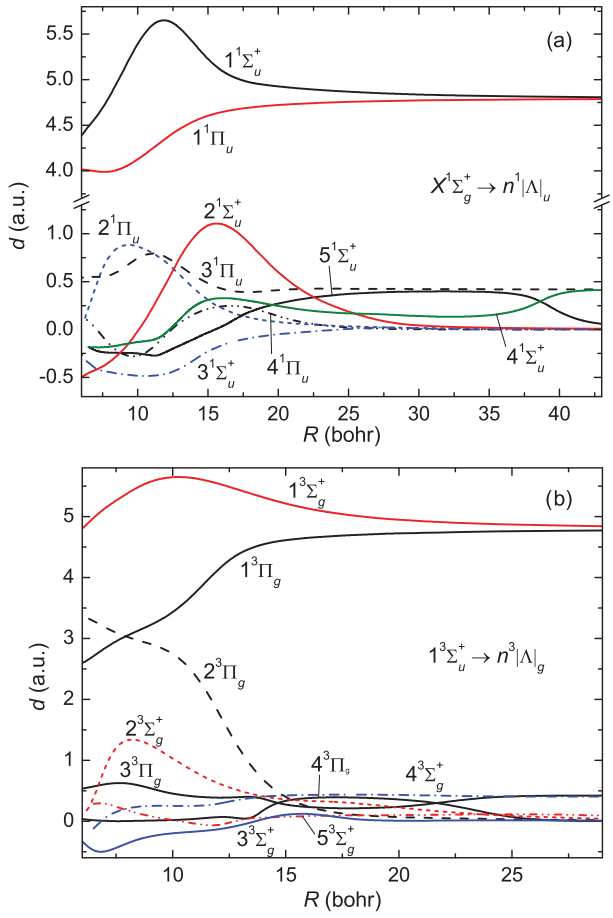

Figure 8. Electric dipole transition moments: (*a*) between the $X^1\Sigma_g^+$ ground state and excited states of $^1\Sigma_u^+$ and $^1\Pi_u$ symmetry, and (*b*) between the $a^3\Sigma_u^+$ lowest triplet state and excited states of $^3\Sigma_g^+$ and $^3\Pi_g$ symmetry.

$6000\,a_0^3$. Such large values of both the interaction-induced variation of isotropic and anisotropic polarisabilities suggest that the influence of the non-resonant laser field on the rovibrational dynamics and transitions between the ground $X^1\Sigma_g^+$ state, and the $A^1\Sigma_u^+$ and $b^3\Pi_u$ states, should be significant even at relatively weak field intensities. Comparing the present polarisabilities of the $X^1\Sigma_g^+$ and $a^3\Sigma_u^+$ states with theoretical results by Deiglmayr *et al.* [77], we find good agreement. For example, the isotropic polarisability α given by trace of the polarisability tensor for the $X^1\Sigma_g$ and $a^3\Sigma_u^+$ states is 522 a.u. and 675 a.u. in the present study and 533 a.u. and 678 a.u. in Ref. [77], respectively.

Note parenthetically that the transition moments and matrix elements of the spin-orbit coupling also change when a DC or non-resonant AC field is applied, but the changes induced on the rovibrational spectrum are expected to be smaller compared to the effects introduced within Equation (13). Therefore, the investigation of the field-induced variation of the transition moments and spin-orbit couplings is out of the scope of the present paper.

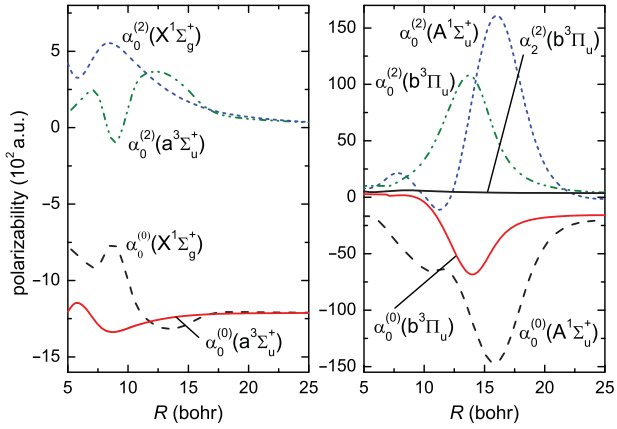

Figure 9. Electric dipole polarisabilities for the electronic ground state (left) and the first excited state (right).

5.4. *Rovibrational spectra in the* $A^1\Sigma_u^+ + b^3\Pi_u$ *manifold without a non-resonant field*

We now compare in more detail the ability of our *ab initio* data to reproduce the fine details of high-resolution experiments of Ref. [35]. In Figure 10(*a*), we report the *ab initio* and empirical potentials for the $A^1\Sigma_u^+$ and $b^3\Pi_u$ states of Rb_2. Inspection of Figure 10(*a*) shows a very good agreement. The *ab initio* calculations reproduce the well depth

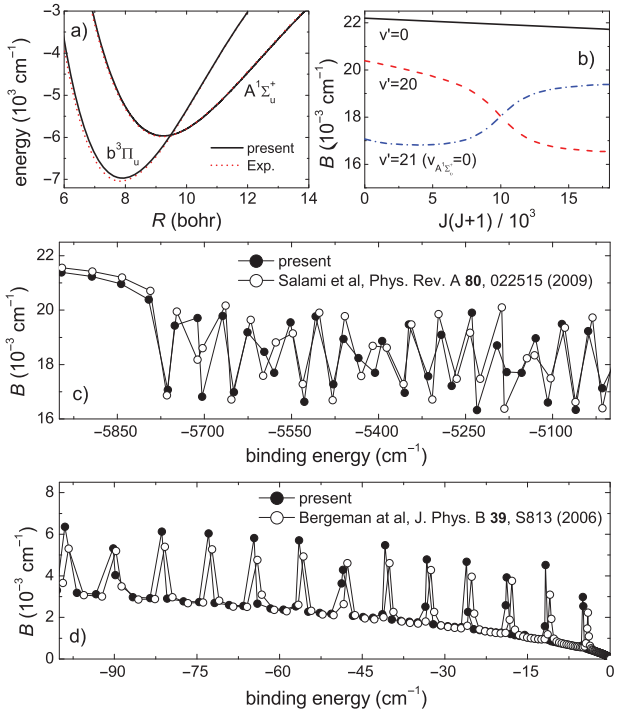

Figure 10. Characteristics of the rovibrational levels for the $|\Omega| = 0_u^+$ component of the coupled $A^1\Sigma_u^+$ and $b^3\Pi_u$ manifold of states in $^{87}Rb_2$: (*a*) present and empirical potential energy curves [35], (*b*) rotational spacings, and $j = 1$ rotational constants for strongly bound levels (*c*) and close to the dissociation limit (*d*).

of the $A^1\Sigma_u^+$ state within 14 cm^{-1} on the overall depth of 5981 cm^{-1}, i.e. within 0.2%. The agreement for the $b^3\Pi_u$ state is slightly less good. The difference in the well depths amounts to 70 cm^{-1} for the well depth of 7039 cm^{-1}. This represents an error of roughly 1%. Such an agreement between theory and experiment should be considered as very good. Also, the crossing of the $A^1\Sigma_u^+$ and $b^3\Pi_u$ potential energy curves is perfectly reproduced. Our dynamical calculations predict the level $v' = 21$ to be the first rovibrational level corresponding to the A state (see the rotational spacings in panel (*b*) of Figure 10). This is one quantum higher than predicted by the experiment [35], but the 70 cm^{-1} disagreement in the well depths fully explains this difference.

Figure 10 also reports the rotational constants for the deeply bound rovibrational levels (panel (*c*)) and levels at the threshold (panel (*d*)). Inspection of Figure 10(*c*) reveals that theory correctly locates all levels that are not perturbed by the spin-orbit interaction, and the first perturbed level. The agreement in the rotational constants for the rovibrational levels in the middle of the potential well is less good, but note the scale on the axis. Overall, we reproduce semi-quantitatively the pattern of the rovibrational levels in this region of the potentials. Also the oscillations of the rotational constants reflecting the perturbations due to the spin-orbit coupling between the $A^1\Sigma_u^+$ and the $b^3\Pi_u$ states are correctly described. This is in accordance with the good agreement between the *ab initio* spin-orbit coupling and the data fitted to the experiment shown in Figure 7. The agreement of the rotational constants for the rovibrational levels near the threshold is very good. This is partly due to the fact that in our calculations we have used the best long-range coefficients from atomic calculations [76]. However, the correct long-range coefficient alone would not be sufficient to obtain such a good agreement between theory and experiment. In fact, panel (*d*) of Figure 10 shows that theory very precisely locates the repulsive walls of the potentials near the zero crossing. This is very gratifying for a theoretical calculation as this region of the potential energy curve is very difficult to describe with *ab initio* methods.

5.5. *Perturbation of the spectra by a non-resonant field*

Bound rovibrational levels are strongly affected by a non-resonant field [55]. We demonstrate in this section that not only are the levels shifted in energy and their rotational motion strongly hybridised, but also, for levels in the coupled $A^1\Sigma_u^+$ and $b^3\Pi_u$ excited state manifold, the singlet-triplet composition may be changed. Note that the non-resonant field mixes different rotational and possibly also vibrational states, and in the presence of the field, v, j, v', j' are not good quantum numbers anymore. However, for simplicity, we do not distinguish between the field-free quantum numbers v, j, v', j' and the corresponding field-dressed labels $\tilde{v}$, $\tilde{j}$, $\tilde{v}'$, $\tilde{j}'$ [55]. The carbon dioxide laser with wavelength of about 10 μm is assumed to be used as a source of a non-resonant field. For that wavelength, the static electric dipole polarisability is good approximation for the dynamic one with a few per cent error both for the ground and excited A+b states.

Comparing three different intensities, Figure 11 illustrates the effect of the non-resonant field on the transition dipole matrix elements for transitions between the $X^1\Sigma_g^+$ ground state and the $A^1\Sigma_u^+$ and $b^3\Pi_u$ excited states. The transition dipole matrix elements are calculated as rovibrational average of Equation (17) for given field-dressed rovibrational levels, i.e. $\sum_{k=A^1\Sigma_u^+, b^3\Pi_u} \langle \varphi^k_{v',j'} | d_z(k \leftarrow X)(R) \cos\theta | \varphi^{X^1\Sigma_g^+}_{v,j} \rangle$, and shown for the $X^1\Sigma_g^+$ state ground level in Figure 11(*a*) and a vibrationally highly excited level in Figure 11(*b*). These levels could be studied using molecules

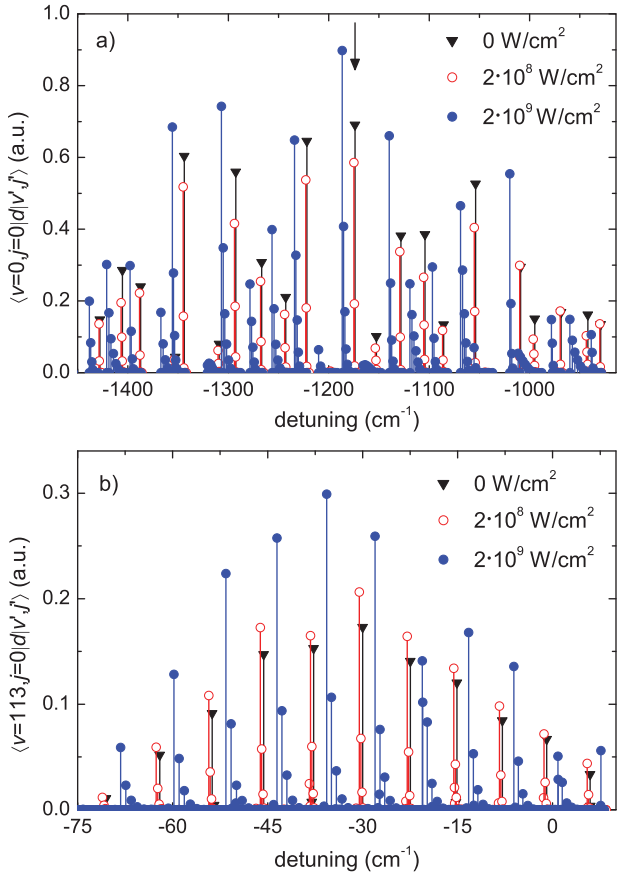

Figure 11. Transition dipole matrix elements between the ground rovibrational level $v = 0, j = 0$ (*a*) and the highly excited level $v = 113, j = 0$ (*b*) of the $X^1\Sigma_g^+$ ground electronic state and rovibrational levels of the $A^1\Sigma_u^+$ and $b^3\Pi_u$ manifold for three intensities of the non-resonant field in $^{87}Rb_2$. The binding energy of the field-free $X^1\Sigma_g^+$ $v = 113$, $j = 0$ level is $E_b = 8.3\,cm^{-1}$. The detuning is computed as $E_{v',J'} - E_{v,J} - (E_{^2P_{1/2}} - E_{^2S})$, with $E_{^2P_{1/2}}$, $E_{^2S}$ the field-free energies of the atomic levels.

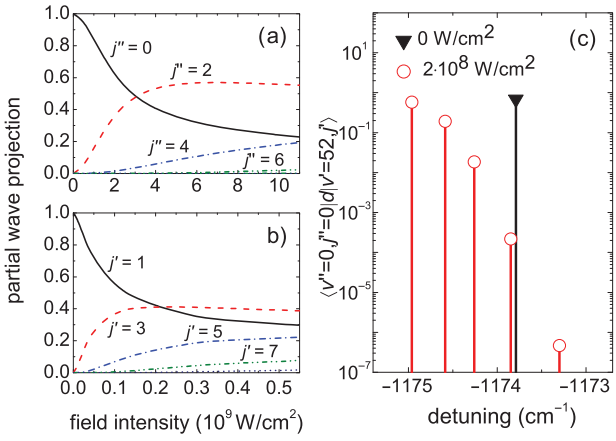

Figure 12. Partial wave decomposition of the field-dressed rovibrational wavefunctions for the $X^1\Sigma_g^+$ state $v = 0, j = 0$ ground level (*a*) and the $v' = 52, J' = 1$ level (*b*) of the $A^1\Sigma_u^+$ and $b^3\Pi_u$ manifold in $^{87}Rb_2$. Also shown are the electric dipole transition moments between the $X^1\Sigma_g^+$ state $v = 0, j = 0$ ground level and the rotational manifold with $v' = 52$ (*c*).

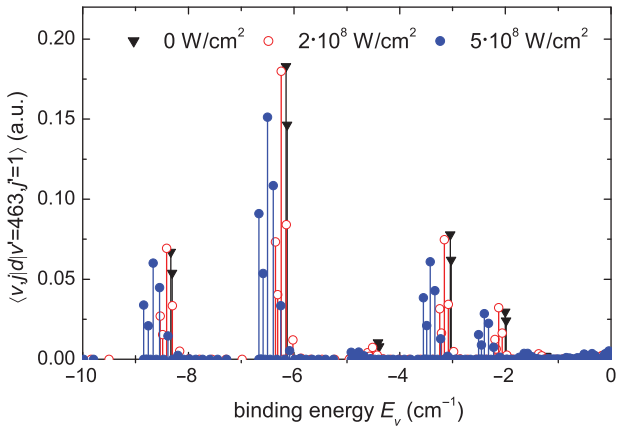

Figure 13. Transition dipole matrix elements for a highly excited rovibrational level ($v' = 463$, $E_{bind}^{v'=463} = 8.3\,\mathrm{cm}^{-1}$) of the $A^1\Sigma_u^+$ and $b^3\Pi_u$ manifold and highly excited $X^1\Sigma_g^+$ state levels in $^{87}Rb_2$.

in a molecular beam (*a*) or produced by photoassociation (*b*) [23]. Inspection of Figure 11 reveals that the transitions get shifted as expected, due to the decrease of all eigenenergies in the non-resonant field [54,55]. Moreoever, the transition strengths are strongly modified. This modification is analysed in more detail in Figure 12 for the strongest transition from the $X^1\Sigma_g^+$ state ground level indicated by an arrow in Figure 11(*a*). Due to hybridisation of the rotational motion, illustrated in Figure 12(*a*) and (*b*) in terms of the projections of the rovibrational wavefunctions onto the field-free partial waves, the wavefunctions consist of contributions from several field-free partial waves between which transitions are allowed. This yields a series of rovibrational lines observed in Figure 12(*c*) instead of the single line for $v = 0, j = 0$ to $v' = 52, j' = 1$ in the field-free case. For the largest intensity shown in Figure 11, $\mathcal{I} = 2 \cdot 10^9\ \mathrm{W/cm^2}$, the transition matrix elements for the strongest lines are clearly larger than in the field-free case. This is rationalised by an alignment of the field-dressed levels in the ground and excited electronic states, with $\langle\cos^2\theta\rangle \gtrsim 0.73$ for $\mathcal{I} = 2 \cdot 10^9\ \mathrm{W/cm^2}$. Correspondingly, the field-dressed wavefunctions are localised in the angular regions θ close to 0 and π. As a consequence, the field-dressed transition strengths are larger than the field-free ones due to the angular dependence of the matrix elements on $\cos\theta$ [78].

Figure 13 illustrates the effect of a non-resonant field on the transition dipole moments for a weakly bound level in the excited $A^1\Sigma_u^+$ and $b^3\Pi_u$ state manifold. This level is particularly well-suited for the photoassociative production of Rb_2 molecules [23], and the analysis of Figure 13 is motivated by a recent proposal for enhancing photoassociation rates using a non-resonant field [55]. While the calculations of Ref. [55] were carried out for Sr_2, a somewhat smaller, albeit still significant, enhancement of the photoassociation rate of about one order of magnitude can be expected for Rb_2 [54]. The non-resonant field will affect the spontaneous decay of the photoassociated molecules, which is governed by the matrix elements shown in Figure 13. The field-free data represents a rotationally resolved equivalent of Figure 3 of Ref. [23]. The binding energy of $8.3\,\mathrm{cm}^{-1}$ in Figure 13 corresponds to the ground state level $v = 113$ (cf. Figure 11(*b*)). A weak non-resonant field splits the two lines originating from the $j' = 1$ level into several ones, similar to Figure 12(*c*). The transition strength for $j = 0$ is almost not affected by the weak field. This behaviour is similar to what has been observed for transitions between weakly bound levels of the strontium dimer [55]. For a strong non-resonant field, the binding energies are shifted and the overall behaviour is similar to Ref. [55]. This implies that a non-resonant field may enhance the photoassociation rate without compromising an efficient stabilisation into bound ground state levels by spontaneous emission as it was observed in Ref. [23].

Finally, Figure 14 analyses the interplay of the spin-orbit coupling and the interaction with the non-resonant field for several of the rovibrational levels of the $A^1\Sigma_u^+$ and $b^3\Pi_u$ manifold studied in Figures 11(*a*), 12 and 13. Surprisingly, the levels from the middle of the well, $v' = 52$, . . ., 56, show a remarkable dependence of the singlet-triplet decomposition on the non-resonant field intensity. On the other hand, the singlet-triplet character of weakly bound levels of the $A^1\Sigma_u^+$ and $b^3\Pi_u$ manifold, shown here for the representative $v' = 463$, is hardly affected. This behaviour can be understood by inspection of the R-dependence of the polarisability components and the spin-orbit coupling matrix elements (cf. Figures 9 and 7). Weakly bound levels have most of their amplitude at internuclear separations larger than $R = 20\,a_0$. The spin-orbit coupling is strong at large internuclear separations and smaller at intermediate separations, while the opposite is true for the polarisability components. A large dependence of the singlet-triplet

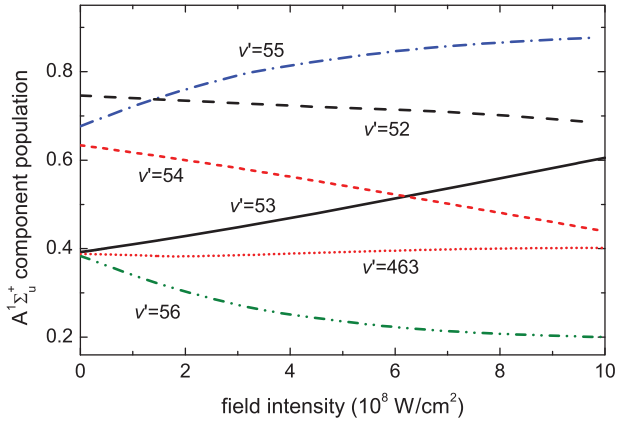

Figure 14. Singlet component of the coupled excited state rovibrational levels versus non-resonant field intensity with v' the field-free vibrational quantum number. Data shown for $j = 1$ (the behaviour for other j is very similar).

character on the non-resonant field intensity is expected when the interaction energy with the field and the spin-orbit coupling become comparable. Due to the R-dependence of the polarisability, for weakly bound levels this requires field intensities in excess of 10^{10} W/cm^2. On the other hand, the more deeply bound levels, $v' = 52, \ldots, 56$, have their outer turning point near $R = 12\,a_0$ where the polarisability is large and the spin-orbit coupling is small. Therefore, intensities of the order of 10^9 W/cm^2 yield an interaction energy with the field that is comparable to the spin-orbit coupling. For example, for 10^9 W/cm^2, the Stark shift of the levels amounts to about 15 cm^{-1}. Their vibrational spacing, of the order of 20 cm^{-1}, is also comparable. The interaction with the non-resonant field will then affect the singlet-triplet character of a rovibrational wavefunction, provided the R-dependence of polarisabilities differs for singlet and triplet states. This is indeed the case, cf. Figure 9, explaining the changes in the singlet-triplet decomposition observed in Figure 14.

6. Summary and conclusions

In the present work, we have investigated how the spectroscopy of the Rb_2 molecule is affected by applying a non-resonant field. Our emphasis has been on the manifold of the spin-orbit coupled $A^1\Sigma_u^+$ and $b^3\Pi_u$ excited states. To this end we have derived the electronic Hamiltonian describing the interaction of a diatomic molecule with a non-resonant field in general and the Hamiltonian describing the nuclear motion in a non-resonant field for the manifold of the coupled $A^1\Sigma_u^+$ and $b^3\Pi_u$ excited electronic states in particular. We have employed the DEA-IH-FS-CCSD for all electronic states of the Rb_2 molecule up to the $5s+5d$ dissociation limit of about 26,000 cm^{-1}. The agreement between the present results and those fitted to high-resolution spectroscopic data is very good, both for the well depths and the vibrational frequencies. The accuracy of the present results for the potential energy curves is much higher than the previous electronic structure calculations in Refs. [40,41] and slightly better than in the most recent study by Allouche and Aubert-Frécon [42].

In order to correctly predict the spectroscopic behaviour, we have also calculated the electric transition dipole moments, non-adiabatic coupling and spin-orbit coupling matrix elements, and static dipole polarisabilities of Rb_2, using the MRCI method. To the best of our knowledge, we have reported in this paper the very first calculation of the irreducible components of the polarisability tensor as a function of R for electronically excited states. For the spin-orbit coupled manifold of the $A^1\Sigma_u^+$ and $b^3\Pi_u$ excited states, we have checked the accuracy of the *ab initio* results with the spectroscopic data. Very good agreement was found.

We have investigated the spectroscopy of Rb_2 in its rovibronic ground state, corresponding to a molecular beam experiment, as well as in highly excited vibrational levels of ground and electronically excited states, typical for photoassociation experiments at ultracold temperatures. In both cases, the spectroscopy is significantly altered by a non-resonant field. Specifically, fields of the order of 10^8 W/cm^2 are found to split a single rovibrational line into several ones and shift the lines by a few cm^{-1}. The splitting is due to rotational hybridisation, i.e. the field-dressed wavefunctions are made up of several field-free partial waves with comparable contributions. For strong non-resonant fields, of the order of 10^9 W/cm^2, alignment leads to an increase of the transition strengths compared to the field-free case, due to localisation of the rotational wavefunctions in regions close to $\theta = 0$ and π, and the dependence of the transition matrix elements on $\cos\theta$ [78]. We have also investigated the effect of a non-resonant field on the transition matrix elements that govern stabilisation by spontaneous emission for photoassociated molecules [23]. Similarly to strontium molecules [55], transitions occur to the same vibrational levels as in the field-free case. This implies that a non-resonant field may be used to enhance the photoassociation rate [55] without deteriorating stabilisation of the photoassociated molecules into bound levels of the electronic ground state. Somewhat surprisingly, we have found a non-resonant field to significantly modify the singlet-triplet character of rovibrational levels in the $A^1\Sigma_u^+$ and $b^3\Pi_u$ excited state manifold for levels in the middle of the potential wells, while weakly bound levels remain rather unaffected. We have identified two conditions for a modification of the singlet-triplet character – the interaction energy with the field needs to be comparable to the spin-orbit coupling and the dependence of the polarisability tensor components on the interatomic separation must differ for singlet and triplet molecules. If both conditions are fulfilled, as was found to be the case for Rb_2 levels of the $A^1\Sigma_u^+$ and $b^3\Pi_u$ manifold with vibrational quantum number around 55, the singlet or triplet

character of a rovibrational wavefunction can be controlled by a non-resonant field.

An interesting perspective for coherent control arises when applying a non-resonant field to degenerate excited electronic states. We have shown that, for degenerate states, a non-resonant field introduces a coupling between different states, 0_u^+ and 2_u in the present example. In coherent control based on wavepacket motion, such a coupling between different states can be used to shape the effective potential energy curve governing the wavepacket dynamics [61]. Using a non-resonant field, for example in the far infrared, comes with the advantage of small losses even for strong fields. Non-resonant field control of photoassociation rates [55] or wavepacket dynamics based on field-induced resonant coupling [61] represents a new twist to manipulating molecules with non-resonant fields [79,80].

Acknowledgements

Financial support from the Polish Ministry of Science and Higher Education through the project N N204 215539 and by the Spanish project FIS2011-24540 (MICINN) as well as the Grants P11-FQM-7276 and FQM-4643 (Junta de Andalucía) is gratefully acknowledged. MT was supported by the project operated within the Foundation for Polish Science MPD Programme co-financed by the EU European Regional Development Fund. RGF belongs to the Andalusian research group FQM-207. RM thanks the Foundation for Polish Science for support within the MISTRZ programme. Part of this work was done while the authors were visitors at the Kavli Institute for Theoretical Physics, University of California at Santa Barbara, within the programme Fundamental Science and Applications of Ultra-cold Polar Molecules. Financial support from the National Science Foundation grant no. NSF PHY11-25915 is gratefully acknowledged.

References

[1] E. Cornell, J. Res. Natl. Inst. Stand. Techol. **101**, 419 (1996).
[2] J.L. Roberts, N. Claussen, J.P. Burke, Jr., C.H. Greene, E.A. Cornell, and C.E. Wieman, Phys. Rev. Lett. **81** (23), 5109 (1998).
[3] E.G.M. van Kempen, S.J.J.M.F. Kokkelmans, D.J. Heinzen, and B.J. Verhaar, Phys. Rev. Lett. **88**, 093201 (2002).
[4] A. Marte, T. Volz, J. Schuster, S. Dürr, G. Rempe, E.G.M. van Kempen, and B.J. Verhaar, Phys. Rev. Lett. **89**, 283202 (2002).
[5] C. Gabbanini, A. Fioretti, A. Lucchesini, S. Gozzini, and M. Mazzoni, Phys. Rev. Lett. **84** (13), 2814 (2000).
[6] S. Dürr, T. Volz, A. Marte, and G. Rempe, Phys. Rev. Lett. **92**, 020406 (2004).
[7] H.M.J.M. Boesten, C.C. Tsai, B.J. Verhaar, and D.J. Heinzen, Phys. Rev. Lett. **77**, 5194 (1996).
[8] H.M.J.M. Boesten, C.C. Tsai, J.R. Gardner, D.J. Heinzen, and B.J. Verhaar, Phys. Rev. A **55** (1), 636 (1997).
[9] T. Volz, S. Dürr, N. Syassen, G. Rempe, E. van Kempen, and S. Kokkelmans, Phys. Rev. A **72**, 010704 (2005).
[10] K. Winkler, G. Thalhammer, M. Theis, H. Ritsch, R. Grimm, and J.H. Denschlag, Phys. Rev. Lett. **95**, 063202 (2005).
[11] F. Lang, K. Winkler, C. Strauss, R. Grimm, and J.H. Denschlag, Phys. Rev. Lett. **101**, 133005 (2008).
[12] M.J. Wright, S.D. Gensemer, J. Vala, R. Kosloff, and P.L. Gould, Phys. Rev. Lett. **95**, 063001 (2005).
[13] M.J. Wright, J.A. Pechkis, J.L. Carini, and P.L. Gould, Phys. Rev. A **74**, 063402 (2006).
[14] M.J. Wright, J.A. Pechkis, J.L. Carini, S. Kallush, R. Kosloff, and P.L. Gould, Phys. Rev. A **75**, 051401 (2007).
[15] J.A. Pechkis, J.L. Carini, C.E. Rogers, P.L. Gould, S. Kallush, and R. Kosloff, Phys. Rev. A **83** (6), 063403 (2011).
[16] J.L. Carini, J.A. Pechkis, C.E. Rogers, P.L. Gould, S. Kallush, and R. Kosloff, Phys. Rev. A **87**, 011401 (2013).
[17] W. Salzmann, T. Mullins, J. Eng, M. Albert, R. Wester, M. Weidemüller, A. Merli, S.M. Weber, F. Sauer, M. Plewicki, F. Weise, L. Wöste, and A. Lindinger, Phys. Rev. Lett. **100**, 233003 (2008).
[18] T. Mullins, W. Salzmann, S. Götz, M. Albert, J. Eng, R. Wester, M. Weidemüller, F. Weise, A. Merli, S.M. Weber, F. Sauer, L. Wöste, and A. Lindinger, Phys. Rev. A **80** (6), 063416 (2009).
[19] A. Merli, F. Eimer, F. Weise, A. Lindinger, W. Salzmann, T. Mullins, S. Götz, R. Wester, M. Weidemüller, R. Ağanoğlu, and C.P. Koch, Phys. Rev. A **80**, 063417 (2009).
[20] D.J. McCabe, D.G. England, H.E.L. Martay, M.E. Friedman, J. Petrovic, E. Dimova, B. Chatel, and I.A. Walmsley, Phys. Rev. A **80**, 033404 (2009).
[21] T. Bergeman, J. Qi, D. Wang, Y. Huang, H.K. Pechkis, E.E. Eyler, P.L. Gould, W.C. Stwalley, R.A. Cline, J.D. Miller, and D.J. Heinzen, J. Phys. B **39**, S813 (2006).
[22] Y. Huang, J. Qi, H.K. Pechkis, D. Wang, E.E. Eyler, P.L. Gould, and W.C. Stwalley, J. Phys. B **39**, S857 (2006).
[23] H.K. Pechkis, D. Wang, Y. Huang, E.E. Eyler, P.L. Gould, W.C. Stwalley, and C.P. Koch, Phys. Rev. A **76**, 022504 (2007).
[24] A. Fioretti, O. Dulieu, and C. Gabbanini, J. Phys. B **40** (16), 3283 (2007).
[25] M.A. Bellos, D. Rahmlow, R. Carollo, J. Banerjee, O. Dulieu, A. Gerdes, E.E. Eyler, P.L. Gould, and W.C. Stwalley, Phys. Chem. Chem. Phys. **13**, 18880 (2011).
[26] P.H. Huber and G. Herzberg, *Molecular Spectra and Molecular Structure: IV. Constants of Diatomic Molecules* (Van Nostrand Reinhold, New York, 1979).
[27] E.O. Lawrence and N.E. Edlefsen, Phys. Rev. **34**, 233 (1929).
[28] J.Y. Seto, R.J.L. Roy, J. Vergès, and C. Amiot, J. Chem. Phys. **113** (8), 3067 (2000).
[29] J. Lozeille, A. Fioretti, C. Gabbanini, Y. Huang, H.K. Pechkis, D. Wang, P.L. Gould, E.E. Eyler, W.C. Stwalley, M. Aymar, and O. Dulieu, Eur. Phys. J. D **39**, 261 (2006).
[30] B. Beser, V.B. Sovkov, J. Bai, E.H. Ahmed, C.C. Tsai, F. Xie, L. Li, V.S. Ivanov, and A.M. Lyyra, J. Chem. Phys. **131**, 094505 (2009).
[31] C. Strauss, T. Takekoshi, F. Lang, K. Winkler, R. Grimm, J. Hecker Denschlag, and E. Tiemann, Phys. Rev. A **82**, 052514 (2010).
[32] M. Mudrich, P. Heister, T. Hippler, C. Giese, O. Dulieu, and F. Stienkemeier, Phys. Rev. A **80**, 042512 (2009).
[33] G. Auböck, M. Aymar, O. Dulieu, and W.E. Ernst, J. Chem. Phys. **132**, 054304 (2010).
[34] R.F. Gutterres, C. Amiot, A. Fioretti, G. Gabbanini, M. Mazzoni, and O. Dulieu, Phys. Rev. A **66**, 024502 (2002).
[35] H. Salami, T. Bergeman, B. Beser, J. Bai, E.H. Ahmed, S. Kotochigova, A.M. Lyyra, J. Huennekens, C. Lisdat, A.V. Stolyarov, O. Dulieu, P. Crozet, and A.J. Ross, Phys. Rev. A **80**, 022515 (2009).
[36] C. Amiot, Mol. Phys. **58** (4), 667 (1986).
[37] C. Amiot and J. Verges, Mol. Phys. **61** (1), 51 (1987).
[38] C. Amiot, J. Chem. Phys. **93** (12), 8591 (1990).
[39] D. Konowalow and M. Rosenkrantz, ACS Symp. Ser. **179**, 3 (1982).

[40] S.J. Park, S.W. Suh, Y.S. Lee, and G.H. Jeung, J. Mol. Spectrosc. **207** (2), 129 (2001).
[41] D. Edvardsson, S. Lunell, and C.M. Marian, Mol. Phys. **101**, 2381 (2003).
[42] A.R. Allouche and M. Aubert-Frecon, J. Chem. Phys. **136** (11), 114302 (2012).
[43] W. Jastrzebski (private communication).
[44] P.L. Gould (private communication).
[45] T. Ban, H. Skenderović, R. Beuc, I.K. Bronić, S. Rousseau, A. Allouche, M. Aubert-Frécon, and G. Pichler, Chem. Phys. Lett. **345**, 423 (2001).
[46] T. Ban, R. Beuc, H. Skenderovi, and G. Pichler, Europhys. Lett. **66** (4), 485 (2004).
[47] M. Tomza, M.H. Goerz, M. Musiał, R. Moszynski, and C.P. Koch, Phys. Rev. A **86**, 043424 (2012).
[48] C.P. Koch, M. Ndong, and R. Kosloff, Faraday Disc. **142**, 389 (2009).
[49] M. Musiał, J. Chem. Phys. **136** (13), 134111 (2012).
[50] R.J. Bartlett and M. Musiał, Rev. Mod. Phys. **79**, 291 (2007).
[51] D.I. Lyakh, M. Musiał, V.F. Lotrich, and R.J. Bartlett, Chem. Rev. **112** (1), 182 (2012).
[52] D. Spelsberg, J. Chem. Phys. **111**, 9625 (1999).
[53] W. Skomorowski and R. Moszynski, J. Chem. Phys. **134** (12), 124117 (2011).
[54] R. Ağanoğlu, M. Lemeshko, B. Friedrich, R. González-Férez, and C.P. Koch, arXiv:1105.0761 (2011).
[55] R. González-Férez and C.P. Koch, Phys. Rev. A **86**, 063420 (2012).
[56] T.G.A. Heijmen, R. Moszynski, P.E.S. Wormer, and A. van der Avoird, Mol. Phys. **89**, 81 (1996).
[57] B. Bussery-Honvault, J.M. Launay, and R. Moszynski, Phys. Rev. A **68**, 032718 (2003).
[58] B. Bussery-Honvault, J.M. Launay, and R. Moszynski, Phys. Rev. A **72**, 012702 (2005).
[59] B. Bussery-Honvault, J.M. Launay, T. Korona, and R. Moszynski, J. Chem. Phys. **125**, 114315 (2006).
[60] B. Bussery-Honvault and R. Moszynski, Mol. Phys. **104** (13–14), 2387 (2006).
[61] C.P. Koch and R. Moszyński, Phys. Rev. A **78**, 043417 (2008).
[62] L. Rybak, S. Amaran, L. Levin, M. Tomza, R. Moszynski, R. Kosloff, C.P. Koch, and Z. Amitay, Phys. Rev. Lett. **107**, 273001 (2011).
[63] L. Rybak, Z. Amitay, S. Amaran, R. Kosloff, M. Tomza, R. Moszynski, and C.P. Koch, Faraday Disc. **153**, 383 (2011).
[64] W. Skomorowski, R. Moszynski, and C.P. Koch, Phys. Rev. A **85**, 043414 (2012).
[65] W. Skomorowski, F. Pawłowski, C.P. Koch, and R. Moszynski, J. Chem. Phys. **136**, 194306 (2012).
[66] M. Krych, W. Skomorowski, F. Pawłowski, R. Moszynski, and Z. Idziaszek, Phys. Rev. A **83**, 032723 (2011).
[67] M. Tomza, F. Pawłowski, M. Jeziorska, C.P. Koch, and R. Moszynski, Phys. Chem. Chem. Phys. **13** (42), 18893 (2011).
[68] S. Boys and F. Bernardi, Mol. Phys. **19**, 553 (1970).
[69] M. Marinescu and A. Dalgarno, Phys. Rev. A **52** (1), 311 (1995).
[70] P. Bunker and P. Jensen, *Molecular Symmetry and Spectroscopy* (NRC Press, Ottawa, 1998).
[71] I.S. Lim, P. Schwerdtfeger, B. Metz, and H. Stoll, J. Chem. Phys. **122** (10), 104103 (2005).
[72] NIST Atomic Spectra Database, <http://physics.nist.gov/PhysRefData/ASD>.
[73] J.F. Stanton, J. Gauss, S.A. Perera, J.D. Watts, A. Yau, M. Nooijen, N. Oliphant, P. Szalay, W. Lauderdale, S. Gwaltney, S. Beck, A. Balkov, D. Bernholdt, K. Baeck, P. Rozyczko, H. Sekino, C. Huber, J. Pittner, W. Cencek, D. Taylor, and R. Bartlett, *ACES II: Computer Program* (Quantum Theory Project, University of Florida, Gainesville, FL, 2006).
[74] H.J. Werner, P.J. Knowles, F.R.M.R. Lindh, M. Schütz, P. Celani, T. Korona, A. Mitrushenkov, G. Rauhut, T.B. Adler, R.D. Amos, A. Bernhardsson, A. Berning, D.L. Cooper, M.J.O. Deegan, A.J. Dobbyn, E.G. F. Eckert, C. Hampel, G. Hetzer, T. Hrenar, G. Knizia, C. Köppl, Y. Liu, A.W. Lloyd, R.A. Mata, A.J. May, S.J. McNicholas, W. Meyer, M.E. Mura, A. Nicklass, P. Palmieri, K. Pflüger, R. Pitzer, M. Reiher, U. Schumann, H. Stoll, A.J. Stone, R. Tarroni, T. Thorsteinsson, M. Wang, and A. Wolf, *MOLPRO, version 2008.1, a Package of ab initio Programs* 2008, <http://www.molpro.net>.
[75] P. Frey, F. Breyer, and H. Holop, J. Phys. B: At. Mol. Phys. **11** (19), L589 (1978).
[76] A. Derevianko, S.G. Porsev, and J.F. Babb, At. Data Nucl. Data Tables **96** (3), 323 (2010).
[77] J. Deiglmayr, M. Aymar, R. Wester, M. Weidemuller, and O. Dulieu, J. Chem. Phys. **129** (6), 064309 (2008).
[78] M. Mayle, R. González-Férez, and P. Schmelcher, Phys. Rev. A **75**, 013421 (2007).
[79] B. Friedrich and D. Herschbach, Phys. Rev. Lett. **74**, 4623 (1995).
[80] M. Lemeshko and B. Friedrich, J. Phys. Chem. A 114, 9848 (2010).